Perlite-SO₃H nanoparticles as an efficient and reusable catalyst for one-pot three-component synthesis of 1,2-dihydro-1-aryl-naphtho[1,2-*e*][1,3]oxazine-3-one derivatives under both microwave-assisted and thermal solvent-free conditions: single crystal X-ray structure analysis and theoretical study

A. Ramazani[a,*], M. Rouhani[a,*], E. Mirhadi[a], M. Sheikhi[b], K. Ślepokura[c] and T. Lis[c]

[a]Department of Chemistry, University of Zanjan, P.O. Box: 45195-313, Zanjan, Iran

[b]Young Researchers and Elite Club, Gorgan Branch, Islamic Azad University, Gorgan, Iran

[c]Faculty of Chemistry, University of Wrocław, 14 Joliot-Curie St., 50-383 Wrocław, Poland

ABSTRACT: A general synthetic route for the synthesis of 1,2-dihydro-1-aryl-naphtho[1,2-*e*][1,3]oxazine-3-one derivatives has been developed using perlite-SO₃H nanoparticles as efficient catalyst under both microwave-assisted and thermal solvent-free conditions. The combination of 2-naphthol, aldehyde and urea enabled the synthesis of 1,2-dihydro-1-aryl-naphtho[1,2-*e*][1,3]oxazine-3-one derivatives in the presence of perlite-SO₃H nanoparticles in good to excellent yields. This method provides several advantages like simple work-up, environmentally benign, and shorter reaction times along with high yields. In order to explore the recyclability of the catalyst, the perlite-SO₃H nanoparticles in solvent-free conditions were used as catalyst for the same reaction repeatedly and the change in their catalytic activity was studied. It was found that perlite-SO₃H nanoparticles could be reused for four cycles with negligible loss of their activity. Single crystal X-ray structure analysis and theoretical studies also were investigated for **4i** product. The electronic properties of the compound have been analyzed using DFT calculations (B3LYP/6-311+G*). The FMO analysis suggests that charge transfer takes place within the molecule and the HOMO is localized mainly on naphthalene and oxazinone rings whereas the LUMO resides on the naphthalene ring.

INTRODUCTION

The use of heterogeneous catalysts [1-3] has received considerable importance in organic synthesis because of their ease of handling, enhanced reaction rates, greater selectivity, simple work-up, and recoverability of catalysts. Among the various heterogeneous catalysts, particularly, perlite nanoparticles has advantages of eco-friendly, low cost, ease of preparation and catalyst recycling [4]. Perlite is an amorphous volcanic glass that has relatively high water content, typically formed by the hydration of obsidian. Because of its low density and relatively low price, many commercial applications for perlite have developed. In the construction and manufacturing fields, it is used in lightweight plasters and mortars, insulation and ceiling tiles, however there are few reports about using perlite as suitable support for catalytic applications [5-8].

Multicomponent reactions (MCRs) [9-13] can be defined as convergent chemical processes where three or more reagents are combined in such a way that the final product retains significant portions of all starting materials. Therefore, they lead to the connection of three or more starting materials in a single synthetic operation with high atom economy and bond-forming efficiency, thereby increasing molecular diversity and complexity in a fast and often experimentally simple fashion [14,15]. For this reason, multicomponent reactions are particularly well suited for diversity-oriented synthesis [16-18] and the exploratory power arising from their conciseness makes

---

*Corresponding authors. E-mail: aliramazani@gmail.com; rouhani.morteza@gmail.com

them also very powerful for library synthesis aimed at carrying out structure-activity relationship (SAR) studies of drug-like compounds, which are an essential part of the research performed in pharmaceutical and agrochemical companies [19,20]. For all these reasons, the development of new multicomponent reactions is rapidly becoming one of the frontiers of organic synthesis.

Aromatic condensed oxazinone derivatives have received considerable attention due to the attractive pharmacological properties associated with their heterocyclic scaffold [21]. Since many of these heterocyclic systems exhibit biological activities such as anti-inflammatory, antiulcer, antipyretic, antihypertensive and antifungal, these derivatives have become an integral part of pharmacologically important heterocyclic compounds [22-26]. Some of them also act as 5-HT ligands [27], DP receptor antagonists [28], integrin antagonists [29], platelet fibrinogen receptor antagonists [30], calmodulin antagonists [31], inhibitors of the transforming growth factor b (TGF-b) signaling pathway [32], soybean lipoxygenase [33], Janus kinase (JAK) and other protein kinases [34]. Moreover, benzo[1,4]oxazin-3-one analogs act as effective potassium channel openers, immunomodulating reagents, and *etc*. [35,36]. This class of heterocyclic compounds has been also used as precursors in the synthesis of phosphinic ligands for asymmetric catalysis [37]. Therefore, aromatic condensed oxazinone derivatives scaffold can be viewed as a 'privileged structure' among pharmaceutical compounds [38,39]. Inspite of their high potential, there are only few reports which describe the synthesis of naphthalene-condensed oxazinone derivatives [40-43]. In general, all these methods require elevated temperature non recyclable catalyst except those reported by Chaskar *et al*. [40]. Besides, a multi-step and cumbersome reaction involving the use of harsh conditions is required for the synthesis of starting materials such as amino alkylnaphthol. Therefore, development of simple, robust and safer methodologies for the synthesis of naphthoxazinone derivatives is of the prime interest for obtaining these products under conditions tolerated by sensitive functional groups from both synthetic and environmental points of view [44].

Microwave chemistry and microwave-assisted organic synthesis (MAOs) are nowadays undeniably effective tools in medicinal chemistry [45]. The availability of safe, single-

mode dedicated microwave units has allowed the incorporation of this new technology into accelerating drug-discovery, hit-to-lead, and lead optimization programs. The development of more economical synthetic routes can ameliorate the overall process since drug discovery is a costly exercise with a high attrition rate [45]. The use of MAOs has been shown to dramatically reduce processing times, increase product yields, and enhance the purity of the product when compared to the conventionally processed experiments [45]. Since there are several manufacturers of professional-grade equipment and a plethora of adapted methods, one can conclude that this interest continues to grow [46].

Motivated by the afore-mentioned findings, and in a continuation of our interest in synthesis of a wide range of heterocyclic systems in our laboratory [47-54], we describe here a facile one-pot three-component synthesis of 1,2-dihydro-1-aryl-naphtho[1,2-*e*][1,3]oxazine-3-one derivatives (**4**) from 2-naphthol (**1**), aldehyde (**2**) and urea (**3**) in the presence of perlite-SO$_3$H nanoparticles as efficient catalyst under both microwave and thermal solvent-free conditions (Scheme 1).

In recent years, computational chemistry has become an important tool for chemists and a well-accepted partner for experimental chemistry [55-58]. Density functional theory (DFT) method has become a major tool in the methodological arsenal of computational organic chemists. In the present work, we investigate the energetic and structural properties of crystal structures of **4i** using DFT calculations. The optimized geometry, frontier molecular orbitals (FMO), detail of quantum molecular descriptors, molecular electrostatic potential (MEP), chemical tensors, natural charge and NBO analysis were calculated.

RESULTS AND DISCUSSION

Recently, it has been reported that multi-component reactions of 2-naphthol (**1**) with benzaldehyde (**2a**) and urea (**3**) in the presence of a number of catalysts and reagents such as H$_2$NSO$_3$H [59], HClO$_4$/SiO$_2$ [60], 2,4,6-trichloro-1,3,5-triazine [61], InCl$_3$ [62] and CH$_3$SO$_3$H [63] afforded uncyclized product (**5a**) in good yields, without any formation of cycloadduct (**4a**) (Scheme 2).

To optimize the reaction conditions to give cycloadduct
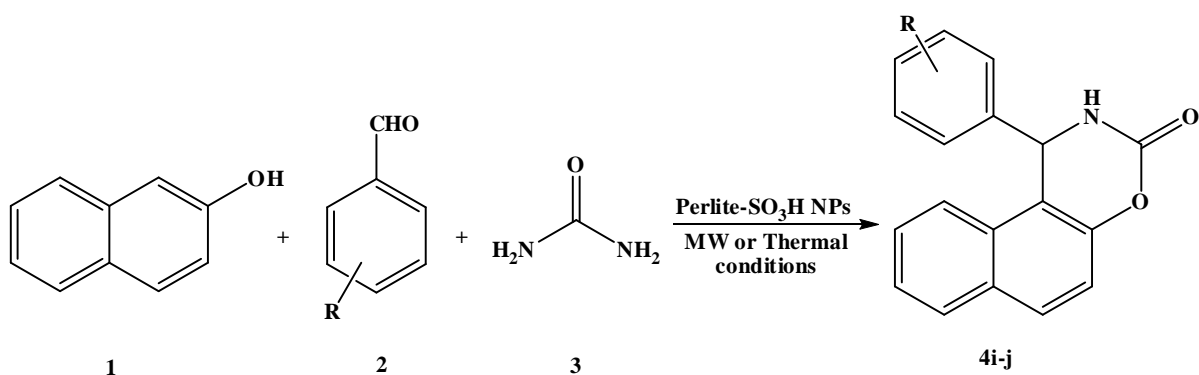
Scheme 1. Synthesis of 1,2-dihydro-1-aryl-naphtho[1,2-*e*][1,3]oxazine-3-one derivatives (**4a-j**)
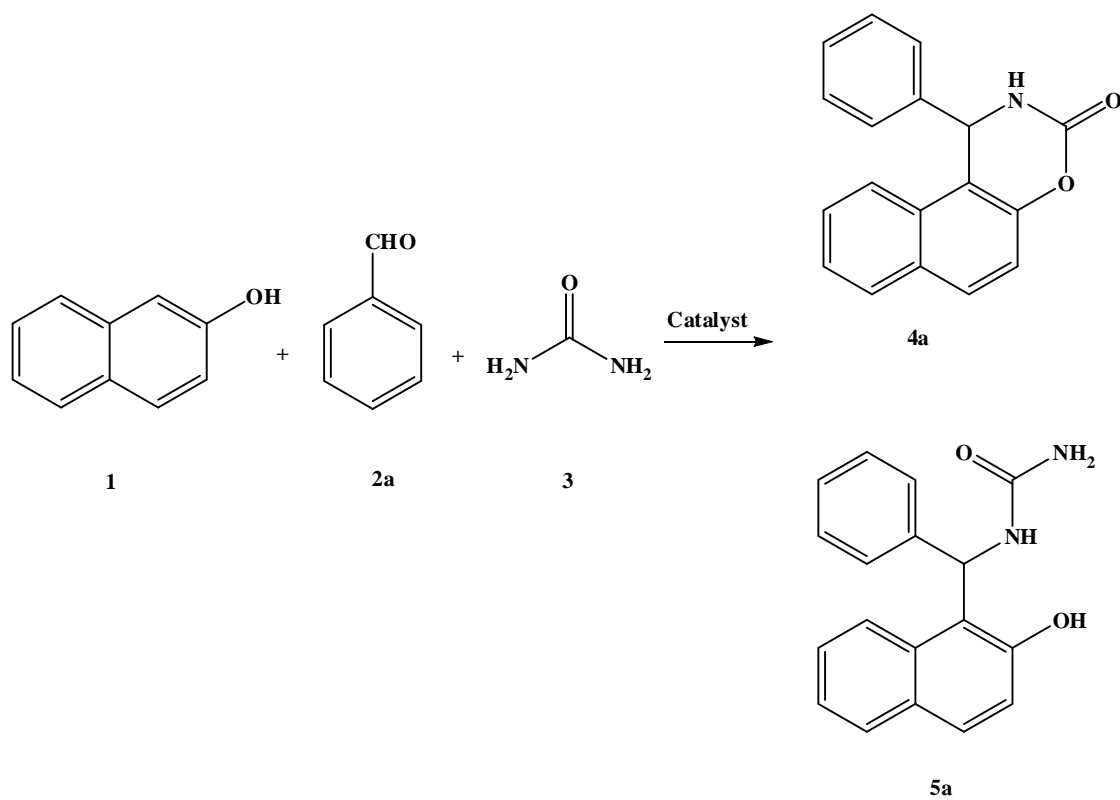
Scheme 2. Possible cyclized and uncyclized products of the reaction

4a, the reaction of 2-naphthol (**1**) with benzaldehyde (**2a**) and urea (**3**) in the presence of various types of perlite as catalyst was used as a model reaction to oxazinone derivatives synthesis. According to the obtained data, using the perlite-SO$_3$H nanoparticles (0.01 g) under solvent-free conditions for the oxazinone formation represents the best reaction conditions (Table 1).

Table 1 clearly demonstrates that perlite-SO$_3$H nanoparticles are an effective catalyst in terms of yield of the obtained product. To find out the optimum quantity of perlite-SO$_3$H nanoparticles, the model reaction was carried out at 110 °C using different quantities of perlite-SO$_3$H nanoparticles (Table 2). According to the obtained data, 0.01 g of perlite-SO$_3$H nanoparticles gave the best yield in 45 min (Table 2, entry 3).

The above reaction was also examined in various solvents (Table 3). The results indicated that different solvents affect the efficiency of the reaction. These solvents

Table 1. Reaction between 2-Naphthol (**1**), Benzaldehyde (**2a**) and Urea (**3**) in the Presence of Various Types of Perlite as Catalyst under Thermal and Solvent-Free Conditions[a]

Entry	Catalyst	Time (min)	Yield (%)
1	Perlite powder	90	10
2	Perlite nanoparticles	60	25
3	Perlite-SO$_3$H nanoparticles	45	53

Table 2. Optimization Amount of perlite-SO$_3$H nanoparticles on the Reaction of 2-Naphthol (**1**), Benzaldehyde (**2a**) and Urea (**3**) under Thermal and Solvent-Free Conditions

Entry	Catalyst (g)	Time (min)	Yield (%)
1	0.1	45	15
2	0.05	45	30
3	0.01	45	53
4	0.005	45	10

required a longer time and gave low to moderate yields, and the best results were obtained when solvent-free conditions were used (Table 3, entry 5).

Encouraged by this success, we attempted the reaction of 2-naphthol (**1**) with a range of other aromatic aldehydes

(**2**) and urea under similar conditions (using perlite-SO₃H nanoparticles), furnishing the respective 1,2-dihydro-1-aryl-naphtho[1,2-*e*][1,3]oxazine-3-one derivatives in good yields. The optimized results are summarized in Table 4. The termal solvent-free conditions are well suited for either

Table 3. Solvent Effect on the Reaction Between 2-Naphthol (**1**), Benzaldehyde (**2a**) and Urea (**3**) under Thermal and Solvent-Free Conditions (0.01 g)

Entry	Solvent	Time	Yield (%)[a]
1	H₂O	24 (h)	20
2	MeOH	24 (h)	30
3	THF	24 (h)	50
4	DMF	24 (h)	No reaction
5	Solvent-free	45 (min)	53

Table 4. Selected Interatomic Distances and Torsion Angles of **4i**

Bond lengths (Å)			
O(1)-C(1)	1.370(2)	N(1)-C(1)	1.332(2)
O(1)-C(4)	1.3980(19)	N(1)-C(2)	1.467(2)
O(2)-C(1)	1.2181(19)	C(2)-C(3)	1.501(2)
Torsion angles (°)			
C(2)-N(1)-C(1)-O(1)	-18.4(2)	C(13)-C(2)-C(3)-C(4)	101.27(17)
C(4)-O(1)-C(1)-N(1)	-7.4(2)	C(13)-C(2)-C(3)-C(12)	-77.21(17)
C(1)-N(1)-C(2)-C(3)	32.44(19)	C(1)-O(1)-C(4)-C(3)	15.3(2)
C(1)-N(1)-C(2)-C(13)	-92.86(18)	N(1)-C(2)-C(13)-C(18)	-110.68(16)
N(1)-C(2)-C(3)-C(4)	-22.52(18)	C(3)-C(2)-C(13)-C(18)	127.03(16)
N(1)-C(2)-C(3)-C(12)	159.00(13)	C(15)-C(16)-C(19)-C(20)	-64.5(2)
		C(15)-C(16)-C(19)-C(21)	171.36(17)

electron-donating or electron-withdrawing substituents on the aromatic aldehydes.

Crystal Structure of 4i

Centrosymmetric crystals of **4i** (space group $P2_1/n$) contain racemic **4i** compound. The molecular structure of (*S*)-enantiomer is shown in Fig. 1. A summary of the conditions for the data collection and the structure refinement parameters are given in *Experimental Part*. The selected geometrical parameters are given in Table 4.

In **4i** molecule, the bond lengths and angles are within normal ranges [64], and the overall conformation of **4i** is very similar to those observed in previously reported 1-phenyl, 1-(4-fluorophenyl) and 1-(4-chlorophenyl) derivatives [65-67]. The six-membered ring O(1)/C(1)/N(1)/C(2)/C(3)/C(4) is slightly puckered (Cremer & Pople [68] amplitude Q = 0.280(2) Å). The mutual orientation of the planar regions, *i.e.* phenyl and naphthalene moieties, is defined by the dihedral angle between them, which is 77.6(1)°, and by the torsion angle

C(13)-C(2)-C(3)-C(12) amounting to -77.21(17)°.

In the crystal lattice of **4i**, the adjacent molecules of the same chirality, related by the action of the 2_1 screw axis, are joined to each other *via* N(1)-H(1*N*)···O(2)[i] hydrogen bondsand weak C(17)-H(17)···O(1)[ii] interactions to form homochiralchains running down the *b*-axis (Fig. 5; geometry and symmetry codes therein). The inter-chain contacts are provided by the weak π···π interactions involving C(3)/C(4)/C(5)/C(6)/C(7)/C(12) rings of the adjacent molecules related by the inversion [centroid···centroid[iii] distance of 3.652(2) Å, centroid···plane perpendicular distance of 3.567(1)Å; symmetry code (iii) -*x*,-*y*+1,-*z*+1].

Also in order to decrease the reaction time, microwave irradiation under solvent-free conditions was used. The reaction time decreased from almost 1 h to a few minutes. Moreover, the yields of products increased in all cases examined (Table 5).

A plausible mechanism for the formation of 2-dihydro-1-aryl-naphtho[1,2-*e*][1,3]oxazine-3-one derivatives in the
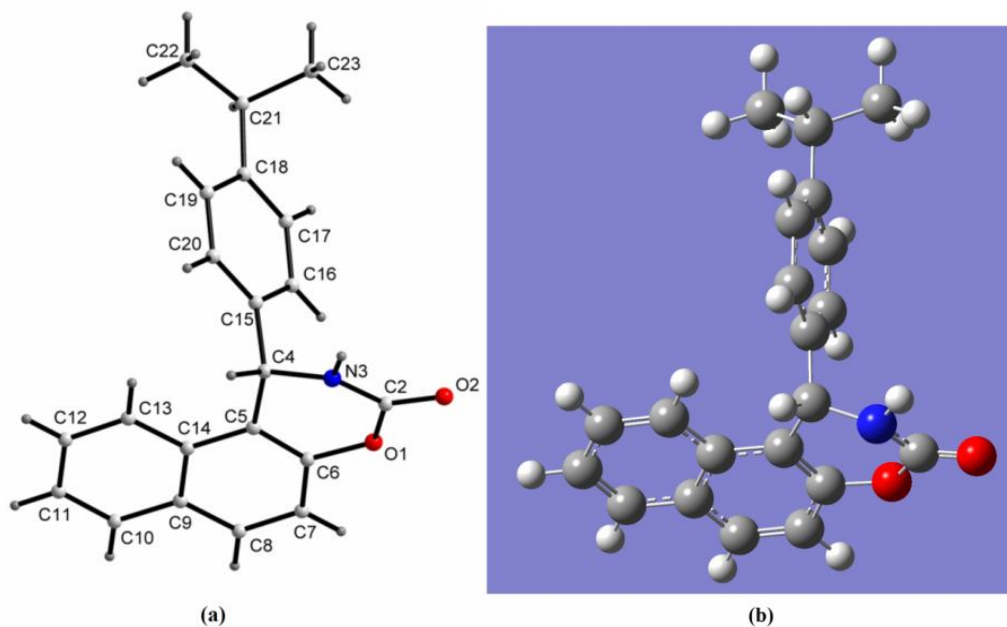

Fig. 1. (a) X-Ray crystal structure of (S)-enantiomer of **4i** compound (displacement ellipsoids at 50% probability level), (b) Geometrical structure of the **4i** compound (optimized at B3LYP/6-311+G* level).
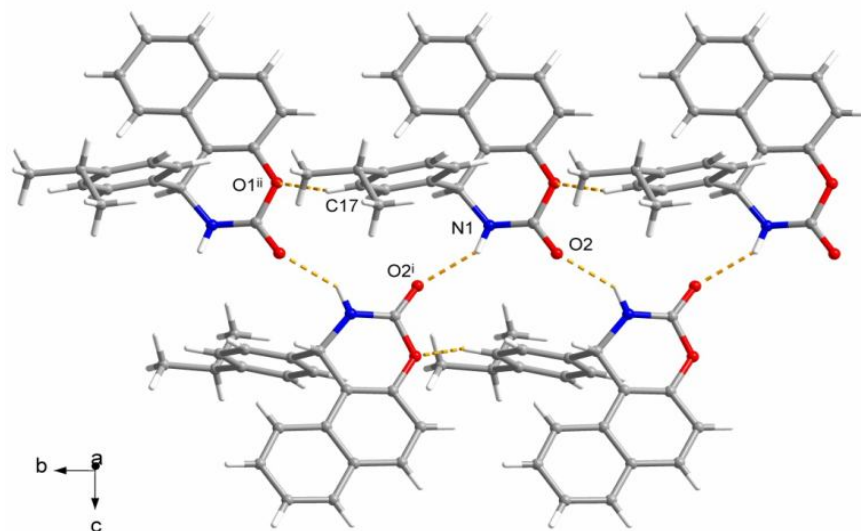
Fig. 2. Molecules of **4i** joined to each other *via* N/C-H···O contacts (dashed lines) to form homochiralchains running down the b-axis. [H···A, D···A, and D–H···A for N(1)-H(1N)···O(2)[i]: 2.08(2), 2.807(2) Å and 143(2)°; for C(17)–H(17)···O(1)[ii]: 2.58, 3.187(2) Å and 122°. Symmetrycodes (i) -x+1/2, y+1/2, -z+3/2; (ii) x, y+1, z].

Table 5. Reaction Between 2-Naphthol (**1**), Aromatic Aldehydes (**2**) and Urea (**3**) under Solvent-Free (I) and Microwave-Assisted[a] (II) Conditions Using 0.01 g Perlite-SO₃H NPs as Catalyst

| Entry	Product	Ar	Time (min)		Yield (%)[b]		M.p. (°C)	
			I	II	I	II	Found	Reported/Ref.
1	**4a**	Ph	50	2	53	87	216-217	217-219/[44]
2	**4b**	4-ClC₆H₄	40	5	60	89	210-211	210-212/[63]
3	**4c**	3-ClC₆H₄	50	2	52	80	110	-
4	**4d**	2,3-Cl₂C₆H₄	50	3	54	79	235-237	-
5	**4e**	4-BrC₆H₄	50	2	65	92	219-220	218-220/[44]
6	**4f**	3-BrC₆H₄	50	2	54	87	118	-
7	**4g**	4-MeC₆H₄	50	2	57	86	171-172	170-172/[64]
8	**4h**	4-MeOC₆H₄	50	3	52	83	187-188	186-188/[44]
9	**4i**	4-(CH₃)₂CHC₆H₄	50	2	53	75	205-207	-
10	**4j**	4-NO₂C₆H₄	60	10	45	85	198-200	205-207/[44]

[a]With a power of 900W. [b]Isolated Yields.

presence of perlite-SO$_3$H nanoparticles is shown in Scheme 3. It may be proposed that similar to several classical multi-component condensations, the initial event in this reaction is the condensation of aldehyde and urea to give reactive acylimine intermediate. Subsequently, the resulting acylimine intermediate undergoes a cyclization with 2-naphthol affording the corresponding products and ammonia [69,70].

In order to explore the recyclability of the catalyst, the perlite-SO$_3$H nanoparticles in solvent-free conditions were used as a catalyst for the same reaction repeatedly and the change in their catalytic activity was studied. The relation between the number of cycles of the reaction and the catalytic activity in terms of yield of the products is presented in Fig. 3. It was found that perlite-SO$_3$H nanoparticles could be reused for four cycles with negligible loss of their activity.

Electronic Properties and MEP Analysis

Quantum chemical methods are important to obtain
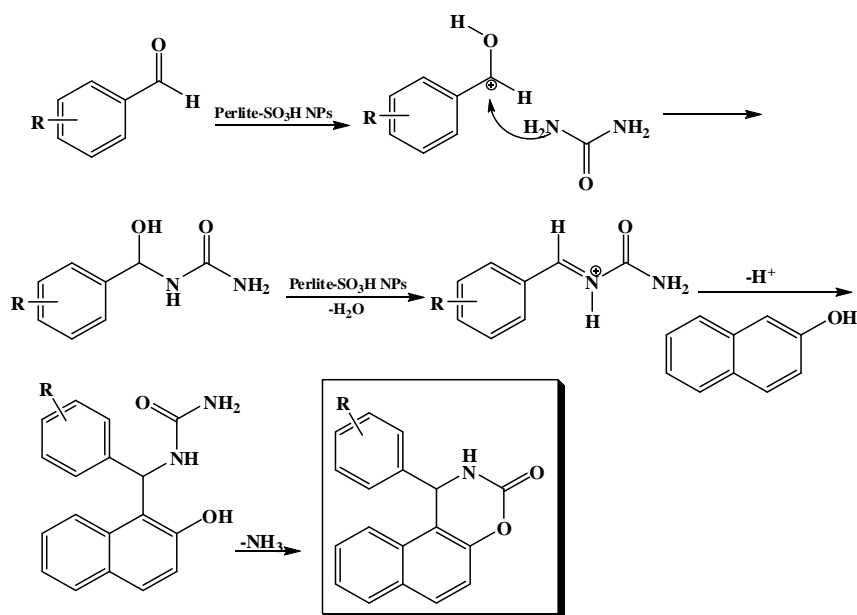
Scheme 3. A proposed mechanism for the synthesis of 2-dihydro-1-aryl-naphtho[1,2-*e*][1,3]oxazine-3-one derivatives in the presence of perlite-SO$_3$H nanoparticles.
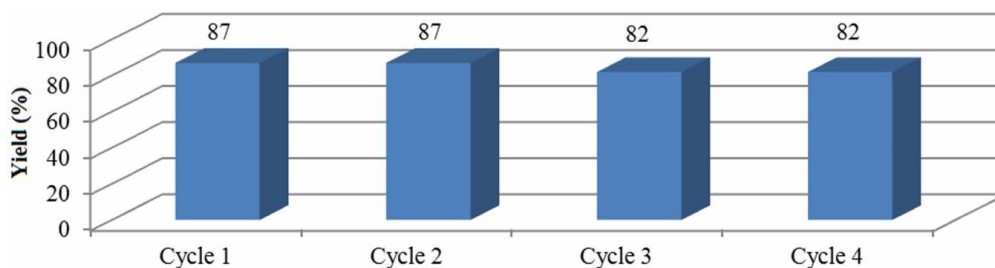
Fig. 3. Development of the yield after several recycling cycles of the catalyst.

information about molecular structure and electrochemical behavior. The Frontier Molecular Orbitals (FMO) analysis was carried out for **4i** compound at B3LYP/6-311+G* level [71]. The results of FMO such as E_{HOMO}, E_{HOMO-1}, E_{LUMO}, E_{LUMO+1} and HOMO-LUMO energy gap (E_g) of the molecule **4i** are summarized in Table 6.

The energy values of the highest occupied molecular orbital (E_{HOMO}) can act as an electron donor and the lowest unoccupied molecular orbital (E_{LUMO}) can act as the electron acceptor and their energy gaps reflect the chemical activity of the molecule [72]. As shown in Fig. 4 and Table 6, E_{HOMO} and E_{LUMO} of the title compound is -6.3 eV and -1.68 eV, respectively. As seen in Fig. 4, charge transfer takes place within the molecule. The graphic pictures of HOMO and LUMO orbitals show that the HOMO of **4i** molecule is localized mainly on naphthalene and oxazinone rings,

Table 6. Calculated (B3LYP/6-311+G*) HOMO, LUMO, Energy Gaps (HOMO-LUMO) and Related Molecular Properties of **4i** Molecule

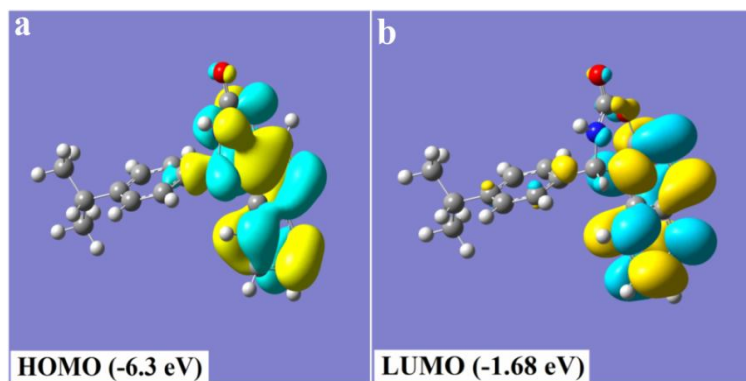| Property	Value
Energy (Hatree-Fock)	-1017.154
μ_D (Debye)	5.567
E_{HOMO} (eV)	-6.3
E_{LUMO} (eV)	-1.68
E_{HOMO-1} (eV)	-6.89
E_{LUMO+1} (eV)	-0.97
Energy gap (E_g) (eV)	4.62
Ionisation potential ($I = -E_{HOMO}$) (eV)	6.3
Electron affinity ($A = -E_{LUMO}$) (eV)	1.68
Chemical potential ($\mu = -(I + A)/2$) (eV)	-3.99
Global hardness ($\eta = (I - A)/2$) (eV	2.31
Global electrophilicity ($\omega = \mu^2/2\eta$) (eV)	3.44

Fig. 4. Calculated frontier molecular orbitals HOMO (a) and LUMO (b) of structure **4i.**

whereas the LUMO is focused mainly on naphthalene ring. The HOMO → LUMO transition implies an electron density transfer from oxazinone to naphthalene ring.

Also in this work, electronic structure of the **4i** compound was studied using total densities of states (DOSs) [73]. DOS plot shows population analysis per orbital and demonstrates a simple view of the character of the molecular orbitals in a certain energy range [74]. According to Fig. 5, DOS analysis indicates that the calculated HOMO-LUMO energy gap (Eg) of the **4i** molecule is 4.62 eV.

A detail of quantum molecular descriptors of **4i** structure such as the ionization potential (*I*), electron affinity (*A*), chemical hardness (*η*), electronic chemical potential (*μ*) and electrophilicity (*ω*) are summarized in Table 6. Dipole moment (*μ_D*) is a good measure for the asymmetric nature of a structure [71]. The size of the dipole moment depends on the composition and dimensionality of the 3D structures. As shown in Table 6, dipole moment of the title structure is 5.567 Debye that the high value of dipole moment is due to its asymmetric character that the atoms are irregularly arranged which gives rise to the increased dipole moment. In addition, the point group of structure is C1 (see Table 6).

The molecular electrostatic potential (MEP) was checked out by theoretical calculations at B3LYP/6-311+G*

level. Molecular electrostatic potential shows the electronic density and is useful in recognition sites for electrophilic attack and nucleophilic reactions as well as hydrogen bonding interactions [75,76]. The negative areas (red color) of MEP are related to electrophilic reactivity and the positive areas (blue color) to nucleophilic reactivity shown in Fig. 6. Molecular electrostatic potential V(r) [77] value is -8.930e^-2. According to the MEP maps in Fig. 6, negative region of **4i** compound is mainly focused over the oxygen in C=O group (more color intensity), therefore it is useful region for nucleophilic activity. In addition, the lowest electron density with the highest intensity blue color is observed for the hydrogen atom in N-H, therefore it is suitable site for electrophilic attraction.

Atomic Charge

We calculated the charge distributions for the equilibrium geometry of **4i** molecule by Natural Bond Orbital (NBO) analysis (natural charge) [71,78] at B3LYP/6-311+G* level. The total charge of the investigated molecule is equal to zero. According to Fig. 7, the results of the NBO analysis reveal that the highest positive charge belongs to C_{12} atom in the carbonyl group (0.923e), while the highest value of negative charge is on the N_{13} atom (-0.650e). In addition, oxygen atoms have
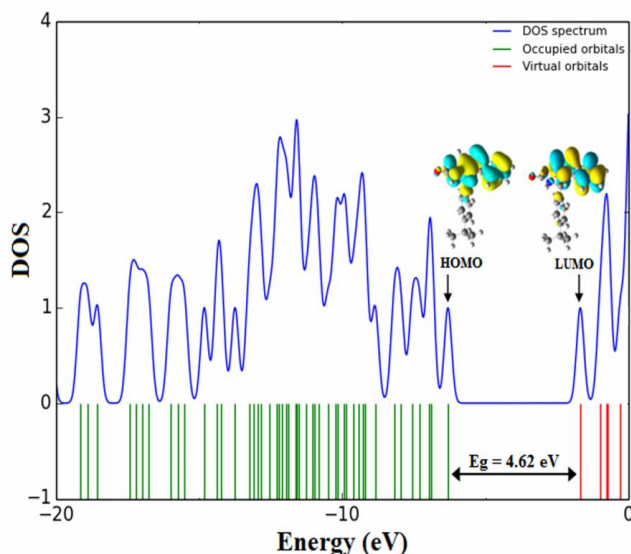

Fig. 5. Calculated DOS plots of **4i** structure (usingB3LYP/6-311+G*).

great negative charge (-0.603e and -0.539e). The carbon atoms of the naphthalene ring bear negative charges except C$_9$ atom (close to oxygen atom) that bear positive charge (0.333e), while the carbon atoms of the phenyl ring bear negative charges. All hydrogen atoms have positive charge

and the H$_{31}$ atom in N-H group has the highest positive charge (0.403e).

The NMR parameters of **4i** molecule are summarized in Table 7. The C$_{23}$ and C$_{24}$ (methyl groups) have the highest σ_{iso} value (158.160 ppm and 157.488 ppm, respectively),
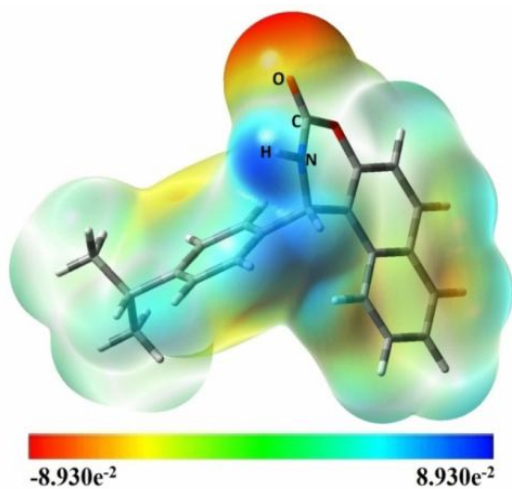

Fig. 6. Molecular electrostatic potential (MEP) maps of **4i** molecule calculated at B3LYP/6-311+G* level.
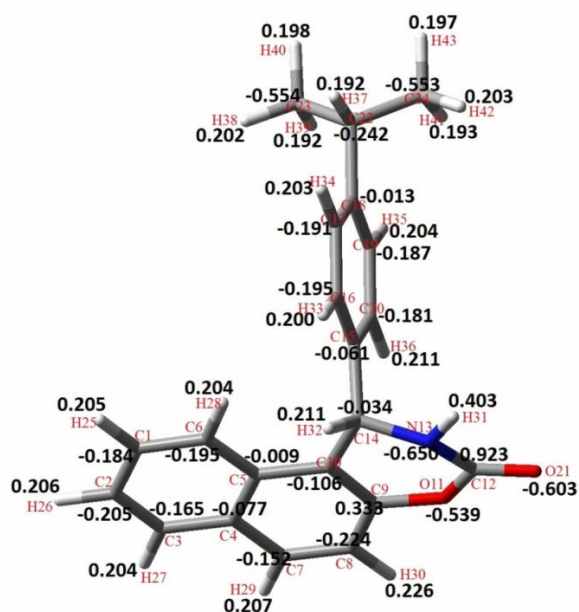

Fig. 7. Calculated (B3LYP/6-311+G*) natural charges (NBO) of the atoms of **4i** molecule. (The Cartesian coordinates of the optimized structure are available in the supplementary material.).

therefore they are shielder than other atoms due to hyperconjugation effect. While O_{21} has the lowest σ_{iso} value (15.809 ppm) and the highest σ_{aniso} value (368.673 ppm) indicating that O_{21} is deshielder than other atoms. According to Table 7, the σ_{iso} value of H_{31} in N-H group is

28.024 ppm that it is shielder than other hydrogen atoms. The σ_{iso} value of C_8, C_9 and C_{10} in naphthalene ring is 61.439 ppm, 26.227 ppm and 63.745 ppm, respectively. It shows the C_9 atom is deshielder than the C_8 and C_{10} atoms, because the C_9 atom is close to the oxygen atom (O_{11}). The

Table 7. The NMR Parameter Values (ppm) of **4i** at B3LYP/6-311+G* Level (Atom Labeling Corresponds to Fig. 7)

Atoms	σ_{iso}	σ_{aniso}	σ_{11}	σ_{22}	σ_{33}
C_8	61.439	148.483	-29.251	53.110	160.428
C_9	26.227	115.853	-59.743	34.962	103.462
C_{10}	63.745	150.246	-11.722	39.048	163.909
O_{11}	111.970	152.152	-6.869	129.374	213.404
C_{12}	31.158	85.508	-62.895	68.205	88.163
N_{13}	142.509	80.388	84.439	146.986	196.101
C_{14}	120.416	18.273	110.190	118.460	132.598
C_{15}	34.305	190.327	-57.467	-0.807	161.190
C_{16}	51.738	156.924	-51.986	50.845	156.354
C_{17}	49.950	152.875	-52.352	50.337	151.867
C_{18}	26.033	208.813	-62.743	-24.399	165.242
O_{21}	15.809	368.673	-142.092	-72.072	261.591
C_{23}	158.160	35.295	143.106	149.685	181.690
C_{24}	157.488	36.210	142.605	148.230	181.628
H_{30}	24.835	5.801	20.434	25.368	28.703
H_{31}	28.024	7.820	20.746	30.089	33.238
H_{32}	26.316	6.502	22.692	25.605	30.651
H_{33}	24.908	7.380	21.886	23.009	29.827
H_{34}	24.956	6.927	21.294	23.999	29.574
H_{35}	25.080	10.549	20.650	22.476	32.112
H_{36}	25.070	11.936	20.097	22.086	33.028

σ_{iso} values of C_{15}, C_{16}, C_{17} and C_{18} atoms in phenyl ring are 34.305 ppm, 51.738 ppm, 49.950 ppm and 26.033 ppm, respectively. As shown, the C_{16} atom is shielder than other and the C18 atom is deshielder than other carbon atoms of phenyl ring.

NBO Analysis

Natural bond orbital (NBO) analysis is an important method for studying interaction between bonds.[79,80] The results of NBO analysis such as the occupation numbers with their energies for the interacting NBOs and the polarization coefficient of atoms for **4i** structure at B3LYP/6-311+G* level are summarized in Table 8. The size of polarization coefficients shows the importance of the two hybrids in formation of the bond. In **4i** structure, the calculated bonding orbital for the C_{12}-N_{13} bond is BD(1) = $0.6169sp^{1.82}$ + $0.7870sp^{1.89}$ with high occupancy 1.98987 a.u. and energy -0.85022 a.u.. The polarization coefficients of C_{12} = 0.6169 and N_{13} = 0.7870 suggest that N_{13} is more electron-rich than the C_{12} atom. The calculated natural

charge (NBO) of N_{13} atom is more negative (-0.650e) than C_{12} atom (0.923e). Thus more the charge density resides on the N_{13}. The calculated bonding orbital for the C_{12}-O_{21} is BD(1) = $0.6002sp^{1.71}$ + $0.7999sp^{1.53}$ with high occupancy 1.99197 a.u. and low energy -1.08004a.u.. The polarization coefficient of O_{21}(0.7999) is greater than C_{12}(0.6002) suggesting that O_{21} is more electron-rich (-0.603e) than C_{12} (0.923e). Also, in the bonding orbital of C_9-O_{11} [BD(1)= $0.5642sp^{1.37}$ + $0.8256sp^{2.05}$] with high occupancy 1.98802 a.u. and energy -0.91039 a.u., the polarization coefficient of C_9(0.5642) is greater than O_{11}(0.8256) indicating that O_{11} is more electron-rich (-0.539e) than C_9(0.333e). From the natural hybrid orbitals C_9-O_{11} and C_{12}-O_{21}, the BD(1)C_9-O_{11} occupies a higher energy orbital (-0.91039 a.u.) with low occupation number (1.98802 a.u.) and BD(1)C_{12}-O_{21} occupies a lower energy orbital (-1.08004 a.u.) with high polarization coefficient (1.99197 a.u.). According to the calculated bondin orbital for the N_{13}-H_{31}, C_{14}-H_{32} and C_{22}-H_{37} bonds, the polarization coefficients of N_{13}, C_{14} and C_{22} are greater than that for H atoms indicative of the

Table 8. Calculated Natural Bond orbitals (NBOs) and Polarization Coefficient for Each Hybrid in Selected Bonds of **4i** Compound at B3LYP/6-311+G* Level (Atom Labeling Corresponds to Fig. 7)

Energy (a.u.)	Bond (A-B)[a]	Occupancy (a.u.)	A	B
-0.70472	BD (1) C_8-C_9	1.96967	0.7016 $sp^{1.97}$	0.7126 $sp^{1.72}$
-0.91039	BD (1) C_9-O_{11}	1.98802	0.5642 $sp^{3.46}d^{0.01}$	0.8256 $sp^{1.97}$
-0.89961	BD (1) O_{11}-C_{12}	1.98798	0.8306 $sp^{2.34}$	0.5568 $sp^{2.62}d^{0.01}$
-0.85022	BD (1) C_{12}-N_{13}	1.98987	0.6169 $sp^{1.82}$	0.7870 $sp^{1.89}$
-1.08004	BD (1) C_{12}-O_{21}	1.99197	0.6002 $sp^{1.71}$	0.7999 $sp^{1.53}$
-0.75699	BD (1) N_{13}-C_{14}	1.97990	0.7848 $sp^{1.83}$	0.6197 $sp^{3.76}d^{0.01}$
-0.60087	BD (1) C_{22}-C_{24}	1.97659	0.7179 $sp^{2.80}$	0.6161 $sp^{2.36}$
-0.66460	BD (1) N_{13}-H_{31}	1.98062	0.8389 $sp^{2.81}$	0.5442 s
-0.52141	BD (1) C_{14}-H_{32}	1.96904	0.7802 $sp^{3.62}$	0.6256 s
-0.48408	BD (1) C_{22}-H_{37}	1.96907	0.7730 $sp^{3.99}d^{0.01}$	0.6344 s

[a]A-B is the bond between atoms A and B. (A: natural bond orbital and the polarization coefficient of atom; A-B: natural bond orbital and the polarization coefficient of atom B).

importance of N_{13}, C_{14} and C_{22} in formation of N_{13}-H_{31}, C_{14}-H_{32} and C_{22}-H_{37} bonds compared to H atoms.

Electron donor orbital, acceptor orbital and the interacting stabilization energy resulting from the second-order micro disturbance theory [81] are reported in Table 9. The electron delocalization from the filled NBOs (donors) to the empty NBOs (acceptors) describes a conjugative electron transfer process between them [82]. For each donor (*i*) and acceptor (*j*), the stabilization energy *E*(2) associated with the delocalization *i*→*j* is estimated. The resonance energy (E(2)) detected the quantity of participation of electrons in the resonance between atoms [71]. The results of the NBO analysis, such as resonance energy (E(2)), donor NBO (i) and acceptor NBO (j), for **4i** compound at B3LYP/6-311+G* level are listed in Table 9. According to

this table, the BD(1)N_{13}-H_{31} orbital participates as donor and the anti-bonding BD*(1)C_{10}-O_{14} and BD*(1)O_{11}-C_{12} orbitals act as acceptor and their resonance energies (E(2)) are 1.57 and 4.91, respectively. These values indicate large charge transfer from the BD(1)N_{13}-H_{31} to the anti-bonding orbital of BD*(1)O_{11}-C_{12} [BD(1)N_{13}-H_{31}→BD*(1)O_{11}-C_{12}]. Based on NBO analysis, the LP(1)N_{13} orbital participates as donor and the anti-bonding BD*(1)C_{14}-C_{15}, BD*(1)C_{14}-H_{32} and BD*(1)C_{15}-C_{16} orbitals act as acceptor and their resonance energies (E(2)) are 6.15, 93.29 and 1.54, respectively. These values indicate large charge transfer from the LP(1)N_{13} to anti-bonding orbital of BD*(1)C_{14}-H_{32} [LP(1)N_{13}→BD*(1)C_{14}-H_{32}]. Also, the resonance energies (E(2)) for BD(2)C_{17}-C_{18}→BD*(2)C_{15}-C_{16}, BD(2)C_{17}-C_{18}→BD*(1)C_{22}-C_{23} and BD(2)C_{17}-C_{18}→BD*(1)C_{22}-C_{24} are

Table 9. Significant Donor-Acceptor Interactions and Second Order Perturbation Energies of **4i** Compound Calculated at B3LYP/6-311+G* Level (Atom Labeling Corresponds to Fig. 7)

Donor NBO(i)	Acceptor NBO(j)	E(2)[a] (kcal mol^{-1})	E(j)-E(i)[b] (a.u.)	F(i,j)[c] (a.u.)
BD (1) N_{13}-H_{31}	BD* (1) C_{10}-C_{14}	1.57	1.06	0.039
	BD* (1) O_{11}-C_{12}	4.91	0.99	0.064
BD (2) C_{17}-C_{18}	BD* (2) C_{15}-C_{16}	21.71	0.28	0.070
	BD* (1) C_{22}-C_{23}	2.54	0.63	0.039
	BD* (1) C_{22}-C_{24}	2.62	0.63	0.040
LP (1) O_{11}	BD* (1) C_8-C_9	0.84	1.08	0.027
	BD* (1) C_9-C_{10}	5.69	1.11	0.071
	BD* (1) C_{12}-N_{13}	5.39	1.00	0.066
	BD* (1) C_{12}-O_{21}	1.58	1.19	0.039
LP (1) N_{13}	BD* (1) C_{14}-C_{15}	6.15	0.67	0.061
	BD* (1) C_{14}-H_{32}	93.29	0.66	0.044
	BD* (1) C_{15}-C_{16}	1.54	0.31	0.020
LP (2) O_{21}	BD* (1) O_{11}-C_{12}	33.82	0.58	0.127
	BD* (1) C_{12}-N_{13}	22.27	0.70	0.114

[a]E(2) means energy of hyperconjucative interactions. [b]Energy difference between donor and acceptor I and j NBOs. [c]F(i,j) is the Fock matrix element between i and j NBOs .

21.71, 2.54 and 2.62 kcal mol^{-1}, respectively, showing large charge transfer from BD(2)C$_{17}$-C$_{18}$ to the anti-bonding orbital of BD*(2)C$_{15}$-C$_{16}$.

EXPERIMENTAL

General

All reagents were obtained from Merck (Germany) and

Fluka (Switzerland) and used without further purification. Infrared spectra were recorded on a Jasco 6300 FTIR spectrometer. Melting points were measured on an Electrothermal 9100 apparatus and are uncorrected. The microwave-assisted procedures were carried out in a Milestone Microwave Oven operating at 1600 W. SEM (Philips XL-30 SEM) with an acceleration voltage of 17 kV was used to investigate the size of the nanoparticles.
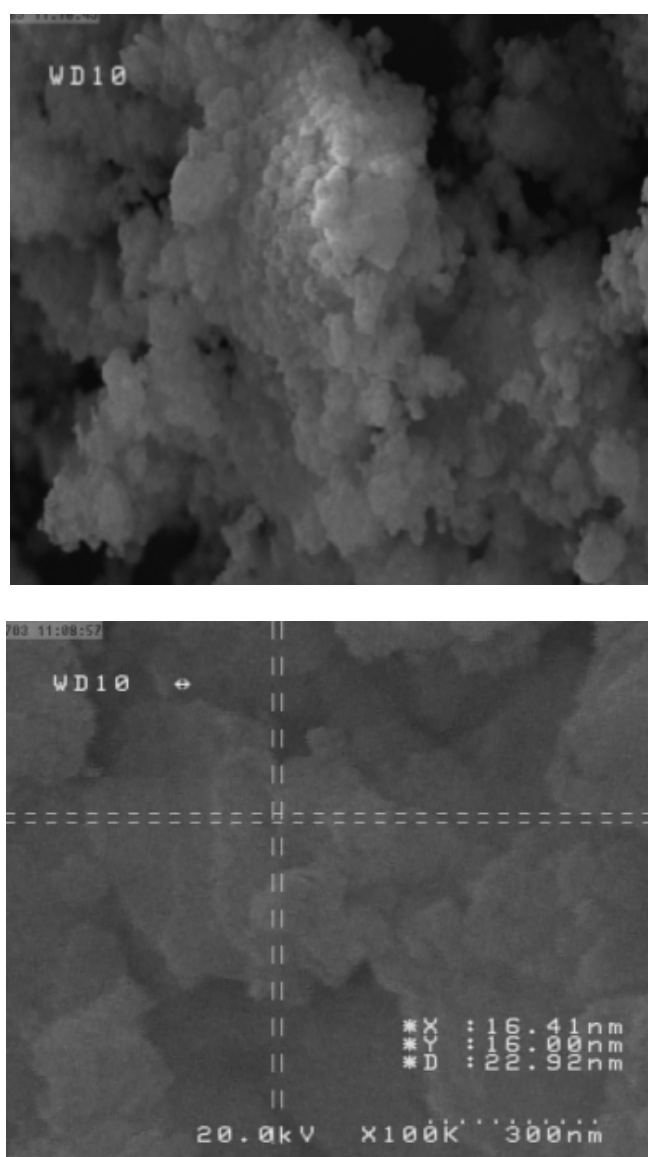
Fig. 8. SEM image of the prepared perlite nanoparticles.

Preparation of the Perlite Nanoparticles

Perlite powder was first broken down to nano size using the ball-milling technique at the frequency of 45 Hz for 20 h under the dry grinding mode. The morphology and grain size of the perlite nanoparticles was investigated by SEM (12 nm) (Fig. 8). The results from X-ray diffraction (XRD) showed that the sample was perlite nanoparticles as indicated by broadened peaks around $2\theta = 26°$ (Fig. 9).

Preparation of the Perlite-SO$_3$H Nanoparticles

Perlite-SO$_3$H nanoparticles, was easily prepared by a simple mixing of the perlite nanoparticles and chlorosulfonic acid at room temperature [83] (Scheme 4). A 250 ml suction flask was equipped with a constant pressure dropping funnel containing chlorosulfonic acid (11.6 g, 0.1 mol) and a gas inlet tube for conducting HCl gas over an adsorbing solution, *i.e.*, H$_2$O. Then, 30.0 g of the perlite nanoparticles was charged into the flask. Chlorosulfonic acid was added drop wise over a period of 30 min at room temperature. After the addition was complete, the mixture was shaken for 30 min. Perlite-SO$_3$H was obtained as a white solid. Surface morphology and particle size were
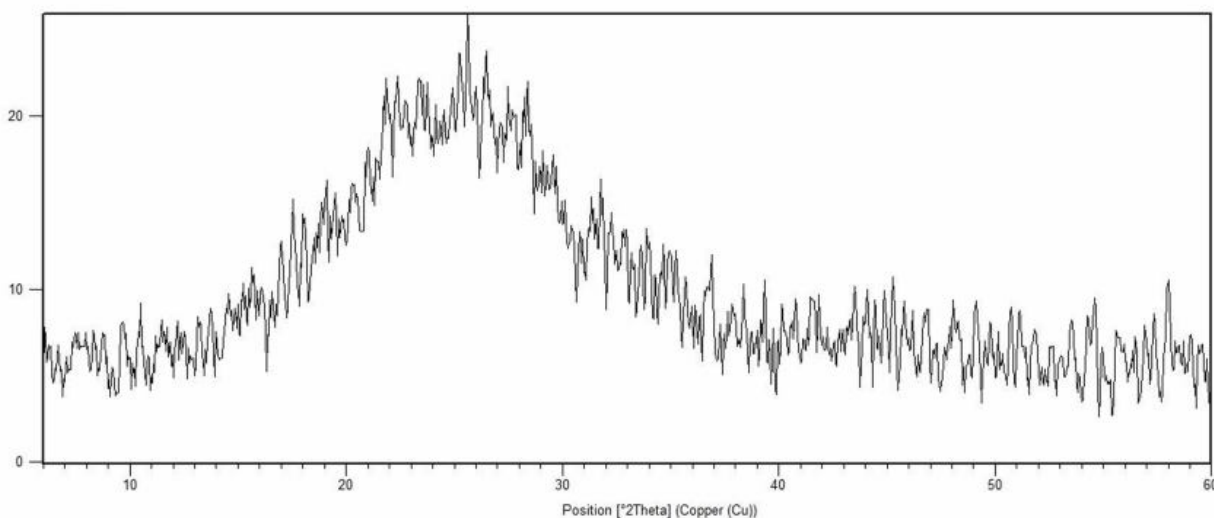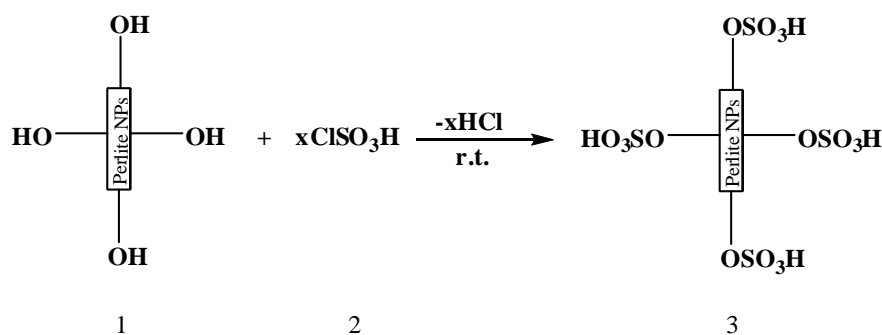

Fig. 9. X-ray diffraction pattern of the prepared perlite nanoparticles.

Scheme 4. Preparation of the perlite-SO$_3$H NPs *via* surface modification of the perlite NPs by chlorosulfonic acid.

obtained using SEM (28 nm) (Fig. 10).

One-Pot Synthesis of 1,2-Dihydro-1-aryl-naphtho[1,2-*e*][1,3]oxazine-3-one derivatives (4a-j) under Thermal Conditions

A mixture of β-naphthol (0.5 mmol), an aromatic aldehyde (0.5 mmol) and urea (0.55 mmol) was heated at 110 °C in the presence of perlite-SO₃H nanoparticles (0.01

g) for the indicated time (Table 1). After completion of the reaction, boiling ethanol was added to the reaction mixture. The catalyst was filtered off and the filtrate was then concentrated and cooled to room temperature. The aqueous ethanol 15% was added to the crude product, the precipitate was separated and then recrystallized using aqueous ethanol 15% twice. The desired pure product(s) was characterized by comparison of their spectroscopical data (FT-IR) and
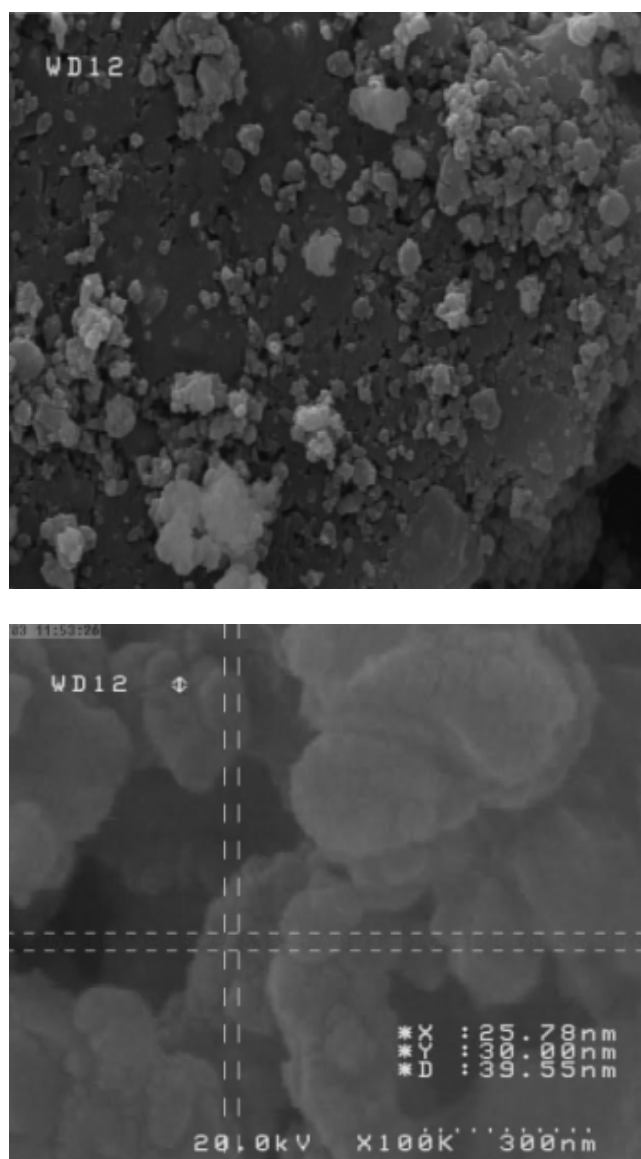

Fig. 10. SEM image of the synthesized perlite-SO₃H nanoparticles.

physical data with those of known oxazine-3-ones (Table 5).

One-Pot Synthesis of 1,2-Dihydro-1-aryl-naphtho[1,2-*e*][1,3]oxazine-3-one Derivatives (4a-j) under Microwave Irradiation

The mixture of β-naphthol (0.5 mmol), an aromatic aldehyde (0.5 mmol) and urea (0.55 mmol) and perlite-SO₃H nanoparticles (0.01 g) was taken in a 50 ml Borosil beaker. The reaction mixture was mixed properly with the help of glass rod and then irradiated in a microwave oven operating power (900 W) for 2-10 min. The progress of the reaction was monitored by TLC, after completion of the reaction; the hot ethanol was added to the reaction mixture and the heterogeneous catalyst was isolated from the mixture by a simple filtration. In continuation of work up, the filtrate ethanol solution was concentrated. The aqueous ethanol (15%) was added to the crude product, the precipitate was separated and then recrystallized using aqueous ethanol (15%) twice. The desired pure product(s) was characterized by comparison of their spectroscopical data (FT-IR) and physical data with those of known oxazine-3-ones.

X-Ray Crystal-Structure Determination of 4i (Fig. 8)

The crystallographic measurement for **4i** CCDC 966112 contains the supplementary crystallographic data for **4i** (These data can be obtained free of charge *via* http://www.ccdc.cam.ac.uk.) was performed at 100(2) K on a Kuma KM4-CCD *κ*-geometry four-circle diffractometer with graphite-monochromatizedMoKα radiation. Data were corrected for *Lorentz* and polarization effects. Data collection, cell refinement, and data reduction and analysis were carried out with the KM4-CCD software, CrysAlis CCD and CrysAlis RED, respectively [84]. Empirical (multi-scan) absorption correction was applied to the data with the use of CrysAlis RED. The structure was solved by direct methods with the SHELXS-2013 program [68], and refined on F^2 by a full-matrix least-squares technique using SHELXL-2013 [68], with anisotropic thermal parameters for the non-H atoms. The H atoms were found in difference Fourier maps, and in the final refinement cycles the C-bonded H atoms were repositioned in their calculated positions and refined using a riding model, with C-H =

0.95-1.00 Å, and with $U_{iso}(H) = 1.2U_{eq}(C)$ for CH, and $1.5U_{eq}(C)$ for CH₃. The N-bonded H atom was refined freely. The figures were made using DIAMOND program [85].

Crystal Ddata for 4i

C₂₁H₁₉NO₂, M = 317.37, yellow plate, crystal size 0.76 × 0.45 × 0.07 mm, monoclinic, space group $P2_1/n$ (no. 14), a = 11.919(3), b = 8.061(2), c = 17.437(4) Å, $β$ = 102.89(3)°, V = 1633.1(7) Å³, T = 100(2) K, Z = 4, $ρ_{calc}$ = 1.291 g cm⁻³, $μ$ = 0.08 mm⁻¹ (for MoKα, $λ$ = 0.71073 Å), T_{min} = 0.943, T_{max} = 1.000, 7272 reflections measured, 3760 unique (R_{int} = 0.028), 2608 observed ($I > 2σ(I)$), $θ$ range 3.1-28.7°, parameters = 223, restraints = 0, R_1 = 0.055, wR_2 = 0.142 (observed refl.), GooF = S = 1.00, largest difference in peak and hole, $Δρ_{max}$ and $Δρ_{min}$ = 0.30 and -0.25 e Å⁻³.

COMPUTATIONAL DETAILS

In this work, to gain a further insight into the properties of **4i**, we have carried out quantum theoretical calculations for this compound at B3LYP/6-311+G* level (DFT) [86-88] by the Gaussian 03W program package [89] . At first, we optimized structure using Gaussian 03W program (see Fig. 1). The electronic properties such as E_{HOMO}, E_{LUMO}, HOMO-LUMO energy gap (Eg), E_{HOMO-1}, E_{LUMO+1}, natural charges, molecular properties, dipole moment ($μ_D$) and point group were detected [90]. The optimized molecular structure, HOMO and LUMO surfaces were visualized using Gauss View 03 program. We also calculated NMR parameters such as chemical shift isotropic (CS^I) and chemical shift anisotropic (CS^A) for title structure [79,91]. Also, the electronic structure of **4i** compound was studied by using Natural Bond Orbital (NBO) analysis at the same level in order to understand various second-order interactions between the filled orbitals of one subsystem and vacant orbitals of another subsystem, which is a measure of the inter-molecular delocalization or hyper conjugation [71,92].

CONCLUSIONS

In conclusion, it can be said that a simple, eco-friendly, green and efficient procedure for the synthesis of

naphthalene condensed oxazinone derivatives from 2-naphthol, aldehydes with urea is reported for the first time by our research group using inexpensive, easily recyclable, and efficient perlite-SO₃H nanoparticles as catalysts in economical and safe, solvent-free in both thermal and microwave conditions. The method is very efficient, avoids the use of expensive reagents, and leads to improved product yields. To the best our knowledge, this is the first report on perlite-SO₃H nanoparticles catalyzed synthesis of naphthaoxazinone derivatives and this new procedure opens an important chapter in the efficient recyclability of perlite-SO₃H nanoparticles as an important catalyst. The ambient conditions, high reaction rates, excellent product yields and easy work-up procedures not only make this methodology an alternative platform to the conventional acid/base catalyzed thermal process but also bring it under the umbrella of environmentally greener and safer synthetic procedures. Additional applications of this technique are currently under investigation. In the present study also, the electronic properties of **4i** compound have been analyzed using DFT calculations (B3LYP/6-311+G*). The FMO analysis suggests that charge transfer takes place within the **4i** molecule and the HOMO is localized mainly on naphthalene and oxazinone rings whereas the LUMO resides on the naphthalene ring. According to the results of NBO analysis, the highest positive and negative charge values belong to carbon atom in carbonyl group (C_{12}: 0.923e), and nitrogen atom (N_{13}: -0.650e), respectvely. NBO nalaysis also show that the polarization coefficients of the electronegative atoms in calculated bonding orbital are greater than electropositive atoms.

ACKNOWLEDGEMENTS

REFERENCES

[1]   G.W. Breton, J. Org. Chem. 62 (1997) 8952.

[2]   M.A. Chari, K. Syamasundar, Catal. Commun. 6 (2005) 67.

[3]   B. Roy, B. Mukopadhya, Tetrahedron Lett. 48 (2007) 3783.

[4]   S.N. Hosseini, S.M. Borghei, M. Vossoughi, N. Taghavinia, Appl. Catalysis–B: Environ. 18 (2007) 53.

[5]   R. Sahraeian, S.A. Hashemi, M. Esfandeh, I. Ghasemi, Polym. Polym. Compos. 20 (2012) 639.

[6]   D.N. Thanh, M. Singh, P. Ulbrich, N. Strnadova, F. Štěpánek, Sep. Purif. Technol. 82 (2011) 93.

[7]   J. Skubiszewska-Zięba, B. Charmas, R. Leboda, V.M. Gun'ko, Micropor. Mesopor. Mat. 156 (2012) 209.

[8]   S. Hasan, T.K. Ghosh, D.S. Viswanath, V.M. Boddu, J. Hazard. Mater. 152 (2008) 826.

[9]   R.V.A. Orru, M. de Greef, Synthesis 10 (2003) 1471.

[10]   D. Tejedor, D. Gonzalez-Cruz, A. Santos-Exposito, J.J. Marrero-Tellado, P. de Armas, F. Garcıa-Tellado, Chem.–Eur. J. 11 (2005) 3502.

[11]   A. Domling, Chem. Rev. 106 (2006) 17.

[12]   G. Guillena, D.J. Ramon, M. Yus, Tetrahedron: Asymmetry 18 (2007) 693.

[13]   B.B. Toure, D.G. Hall, Chem. Rev. 109 (2009) 4439.

[14]   For a monograph on MCRs, see: Multicomponent Reactions; J. Zhu, H. Bienayme, Ed.; Wiley-VCH: Weinheim, (2005).

[15]   For a symposium in print on MCRs, see: Tetrahedron symposium, I. Marek, Ed.; 61 (2005) 11299.

[16]   D.R. Spring, Org. Biomol. Chem. 1 (2003) 3867.

[17]   M.D. Burke, S.L. Schreiber, Angew. Chem. Int. Ed. 43 (2004) 46.

[18]   R.J. Spandl, A. Bender, D.R. Spring, Org. Biomol. Chem. 6 (2008) 1149.

[19]   L. Weber, Curr. Med. Chem. 9 (2002) 2085.

[20]   C. Hulme, V. Gore, Curr. Med. Chem. 10 (2003) 51.

[21]   L. Waxman, P.L. Darke, Antiviral Chem. Chemother. 11 (2000) 1.

[22]   B. Kalluraya, S. Sreenivasa, Farmaco 53 (1998) 399.

[23]   R.D. Larsen, E.G. Corley, A.O. King, J.D. Carrol, P. Davis, T.R. Verhoeven, P.J. Reider, M. Labelle, J.Y. Gauthier, Y.B. Xiang, Y.R.J. Zamboni, J. Org. Chem. 61 (1996) 3398.

[24]   M.P. Maguire, K.R.K. Sheets, A.P. McVety, A. Zilberstein, J. Med. Chem. 37 (1994) 2129.

[25]   Y.L. Chen, K.C. Fang, J.Y. Shen, S.L. Hsu, C.C. Tzeng, J. Med. Chem. 44 (2001) 2374.

[26]   D. Doube, M. Blouin, C. Brideau, C. Chan, S.

Desmarais, D. Eithier, J.P. Falgueyret, R.W. Friesen, M. Girrard, Y. Girard, J. Guay, P. Tagari, Bioorg. Med. Chem. Lett. 8 (1998) 1255.

[27]   K.J. Dougherty, B.A. Bannatyne, E. Jankowska, P. Krutki, D.J.J. Maxwell, Neurosci. 3 (2005) 584.

[28]   M. Iwahashi, K. Kobayashi, F. Nambu, Int. Patent Appl. WO 2003078409 A1, (2003).

[29]   P. Vianello, T.U.S. Bandiera, Patent Appl. US 2003073688A1, (2003).

[30]   M. Anderluh, J. Cesar, P. Stefanic, D. Kikelj, D. Janes, J. Murn, K. Nadrah, M. Tominc, E. Addicks, A. Giannis, M. Stegnar, M.S. Dolenc, Eur. J. Med. Chem. 40 (2005) 25.

[31]   N. Kajino, Y. Shibouta, K. Nishikawa, K. Meguro, Chem. Pharm. Bull. 11 (1991) 2896.

[32]   F.J. Gellibert, A. Payne, Int. Patent Appl. WO 2003097639 A1, (2003).

[33]   D.N. Nicolaides, D.R. Gautam, K.E. Litinas, D. Kikelj, D. Janes, J. Murn, K. Nadrah, M. Tominc, E. Addicks, A. Giannis, M. Stegnar, M.S. Dolenc, J. Heterocycl. Chem. 41 (2004) 605.

[34]   R.S. Bethiel, M.U.S. Ludeboer, Patent Appl. US 2004097504 A1, (2004).

[35]   G. Caliendo, E. Perissutti, V. Santagada, F. Ferdinando, B. Severino, R. d'Emmanuele di Villa Bianca, L. Lippolis, A. Pinto, R. Sorrentini, Bioorg. Med. Chem. 10 (2002) 2663.

[36]   R. Fringuelli, D. Pietrella, F. Schiaffella, A. Guarraci, S. Perito, F. Bistoni, A. Vecchiarelli, Bioorg. Med. Chem. 10 (2002)1681.

[37]   Y. Wang, X. Li, K. Ding, Tetrahedron: Asymmetry 13 (2002) 1291.

[38]   J.F. Austin, D.W.C. MacMillan, J. Am. Chem. Soc. 124 (2002) 1172.

[39]   D.J. Triggle, J. Med. Chem. 3 (2003) 215.

[40]   A. Chaskar, V. Vyahare, V. Padalkar, K. Phatangare, H. Deokar, J. Serb. Chem. Soc. 76 (2011) 21.

[41]   M. Dabiri, A.S. Delbari, A. Bazgir, Synlett 5 (2007) 821.

[42]   A. Nizam, M.A. Pasha, Synthetic Commun. 40 (2010) 2864.

[43]   J. Safaei-Ghomi, S. Zahedi, M.A. Ghasemzadeh, Iran J. Catal. 2 (2012) 27.

[44]   A. Kumar, A. Saxena, M. Dewan, A. Mozumdar, S.

De, Tetrahedron Lett. 52 (2011) 4835.

[45]   C.O. Kappe, A. Stadler, Microwaves in Organic and Medicinal Chemistry; Wiley-VCH: Weinheim, (2005).

[46]   C.O. Kappe, D. Dallinger, S.S. Murphree, Practical Microwave Synthesis for Organic Chemists; Wiley-VCH: Weinheim, (2009).

[47]   A. Ramazani, F. Zeinali Nasrabadi, B. Abdian, M. Rouhani, Bull. Korean Chem. Soc. 33 (2012) 453.

[48]   A. Ramazani, F. Zeinali Nasrabadi, Z. Karimi, M. Rouhani, Bull. Korean Chem. Soc. 32 (2011) 2700.

[49]   A. Ramazani, M. Rouhani, A. Rezaei, N. Shajari, A. Souldozi, Helv. Chim. Acta 94 (2011) 282.

[50]   A. Ramazani, Y. Ahmadi, M. Rouhani, N. Shajari, A. Souldozi, Heteroat. Chem. 21 (2010) 368.

[51]   A. Ramazani, F. Zeinali Nasrabadi, Z. Karimi, M. Rouhani, Synth. Commun. 43 (2010) 1818.

[52]   A. Souldozi, A. Ramazani, Tetrahedron Lett. 48 (2007) 1549.

[53]   A. Souldozi, A. Ramazani, N. Bouslimani, R. Welter, Tetrahedron Lett. 48 (2007) 2617.

[54]   A. Souldozi, K. Ślepokura, T. Lis, A. Ramazani, Z. Naturforsch 62b (2007) 835.

[55]   C.J. Cramer, Essentials of Computational Chemistry: Theories and Models; Wiley, Chichester, (2002).

[56]   a) D. Avci, Y. Atalay, Struct. Chem. 20 (2009) 185; b) R.B. Nazarski, J. Phys. Org. Chem. 22 (2009) 834.

[57]   S.M. Shoaei, A.R. Kazemizadeh, A. Ramazani, Chin. J. Struct. Chem. 30 (2011) 568.

[58]   H. Hopfl, B. Gomez, R. Martinez-Palou, J. Mex. Chem. Soc. 49 (2005) 307.

[59]   R.R. Nagawade, D.B. Shinde, Chin. J. Chem. 25 (2007) 1710.

[60]   B. Das, D.N. Kumar, K. Laxminarayana, B. Ravikanth, Helv. Chim. Acta 90 (2007) 1330.

[61]   P. Zhang, Z.H. Zhang, Monatsh Chem. 140 (2009) 199.

[62]   N.L. Chavan,P.N. Naik, S.K. Nayak, R.S. Kusurkar, Synth. Commun. 40 (2010) 2941.

[63]   V.J. Rani, M. Suresh, P. Lavanya, K.V. Vani, B. Nagarjuna, C.V. Rao, Der Pharma Chemica 2 (2010) 224.

[64]   A. Kumar, M. Sudershan Rao, I. Ahmad, B. Khungar, Can. J. Chem. 87 (2009) 714.

[65] A. Dorehgiraee, H. Khabazzadeh, K. Saidi, Arkivoc vii (2009) 303.

[66] M. Singh, D.N. Thanh, P. Ulbrich, N. Strnadová, F. Štěpánek, J. Solid State Chem. 183 (2010) 2979.

[67] G.B. Dharma Rao, M.P. Kaushik, A.K. Halve, Tetrahedron Lett. 53 (2012) 2741.

[68] D. Cremer, J.A. Pople, J. Am. Chem. Soc. 97 (1975) 1354.

[69] F.H. Allen, O. Kennard, D.G. Watson, L. Brammer, A.G. Orpen, R. Taylor, J. Chem. Soc. Perkin Trans. II (1987) S1.

[70] H.Y. M. Gondal, M. Bhatti, A. Gohar, M. Ali, M.N. Tahir, Acta Cryst. E66 (2010) o2555.

[71] M. Sheikhi, D. Sheikh, A.S. Ramazani, Afr. J. Chem. 67 (2014) 151.

[72] K.G. Vipin Das, C.Y. Panicker, B. Narayana, P.S. Nayak, B.K. Sarojini, A.A. Al-Saadi, Spectrochim Acta A: Mol. Biomol. Spectrosc. 135 (2015) 162.

[73] A. Ahmadi Peyghan, M.T. Baei, M. Moghimi, S. Hashemian, Comput. and Theor. Chem. 997 (2012) 63.

[74] A. Soltani, F. Ghari, A. Dehno Khalaji, F. Tazikeh Lemeski, K. Fejfarova, M. Dusek, M. Sheikhi, Spectrochim. Acta A: Mol. Biomol. Spectrosc. 139 (2015) 271.

[75] H. Tanak, J. Phys. Chem. A, 115 (2011) 13865.

[76] D. Habibi, A.R. Faraji, D. Sheikh, M. Sheikhi, S. Abedi, RSC Adv. 4 (2014) 47625.

[77] P. Politzer, P. Lane, Struct. Chem. 1 (1990) 159.

[78] S. Guidara, H. Feki, Y. Abid, Spectrochim. Acta A: Mol. Biomol. Spectrosc. 133 (2014) 856.

[79] M. Monajjemi, M. Sheikhi, M. Mahmodi Hashemi, F. Molaamin, R. Zhiani, Inter. J. Phys. Sci. 7 (2012) 2010.

[80] F. Weinhold, C.R. Landis, Chem. Educ. Res. Pract. 2 (2001) 91.

[81] B.D. Joshi, P. Tandon, S. Jain, Himalayan Phys. 3 (2012) 44.

[82] E.D. Glendening, A.E. Reed, J.E. Carpenter, F. Weinhold, NBO version 3.1, TCI, University of Wisconsin, Madison, USA, (1998).

[83] M. Mahkam, L. Vakhshouri, Int. J. Mol. Sci. 11 (2010) 1546.

[84] H.R. Khavasi, A. Bazgir, V. Amani, R. Rahimi, J. Chem. Res. 130 (2008) 450.

[85] CCD. CrysAlis CCD and CrysAlis RED in KM4-CCD Software, Oxford Diffraction Ltd, Abingdon, England, (2010).

[86] P.C. Hariharan, J.A. Pople, Theor. Chim. Acta 28 (1973) 213.

[87] P.C. Hariharan, J.A. Pople, Mol. Phys. 27 (1974) 209.

[88] W. Kohn, A.D. Becke, R.G. Parr, J. Phys. Chem. 100 (1996) 12974.

[89] M.J. Frisch, *et al.*, Gaussian 03, revision B03, Gaussian Inc., Pittsburgh, PA, 2003.

[90] A.R. Soltani, M.T. Baei, M. Mirarab, M. Sheikhi, E. Tazikeh Lemeski, J. Phys. Chem. Solids 75 (2014) 1099.

[91] L. Shiri, D. Sheikh, A.R. Faraji, M. Sheikhi, S. Seyed Katouli, Lett. Org. Chem. 11 (2014) 18.

[92] S.A. Seyed Katouli, M. Sheikhi, D. Sheikh, S.F. Tayyari, Orient. J. Chem. 29 (2013) 1121.